ELSEVIER

International Journal of Solids and Structures 40 (2003) 7449–7461

INTERNATIONAL JOURNAL OF SOLIDS and STRUCTURES

www.elsevier.com/locate/ijsolstr

Simulation of ratcheting strain to a high number of cycles under biaxial loading

X. Chen [a], R. Jiao [a], K.S. Kim [b,*]

[a] *School of Chemical Engineering and Technology, Tianjin University, Tianjin 300072, PR China*

[b] *Department of Mechanical Engineering, Pohang University of Science and Technology, San 31 Hyoja-doing, Nam-gu, Pohang 790-784, South Korea*

Received 12 February 2003; received in revised form 8 August 2003

Abstract

The Ohno–Wang kinematic hardening rule is modified to incorporate the Burlet–Cailletaud radial evanescence term for an improved simulation of the ratcheting behavior. The Delobelle parameter δ' is implemented in the modified model to compromise shakedown of the Burlet–Cailletaud hardening rule and over-prediction of the Ohno–Wang model. An evolution equation is proposed for δ' to simulate the ratcheting strain over an extended domain of cycles. Ratcheting tests were conducted on S45C steel under four types of nonproportional axial–torsional loading. The new model is found to yield reasonably accurate predictions of ratcheting strain to a much higher number of cycles compared with other studies.

1. Introduction

When structural components are cyclically loaded in the plastic regime, progressive plastics deformation can occur by a combination of primary (steady) loading and secondary (cyclic) loading. This deformation behavior is referred to as ratcheting. The ratcheting deformation accumulates continuously with the applied number of cycles, and it may not cease until failure.

A number of papers review the state of the art of modeling the ratcheting behavior (Chaboche, 1994; McDowell, 1994; Ohno, 1998; Bari and Hassan, 2000, 2001, 2002). Ratcheting experiments have been conducted on different materials under various loading conditions (Hassan and Kyriakides, 1992; Jiang and Sehitoglu, 1994a; Portier et al., 2000). The studies with existing models indicate that simulation of uniaxial ratcheting primarily depends on the plastic modulus calculation scheme, whereas in multiaxial loading ratcheting depends essentially on the hardening rule employed in the model (Hassan et al., 1992; Hassan and Kyriakides, 1994a,b). Several kinematic hardening rules have been proposed for prediction of ratcheting under multiaxial loading. The conventional linear kinematic hardening rules such as Prager (1956),

* Corresponding author. Tel.: +82-54-279-2182; fax: +82-54-279-5899.
E-mail address: illini@postech.ac.kr (K.S. Kim).

0020-7683/$ - see front matter © 2003 Elsevier Ltd. All rights reserved.
doi:10.1016/j.ijsolstr.2003.08.009

Nomenclature

$\boldsymbol{\alpha}$	deviatoric backstress tensor
$\mathrm{d}\boldsymbol{\alpha}$	incremental deviatoric backstress tensor
$\mathrm{d}p$	magnitude of the incremental plastic strain tensor
$\boldsymbol{n}$	unit normal to the yield surface at current stress point
$\boldsymbol{s}$	deviatoric stress
E	Young's modulus for elasticity
G	shear modulus
H	plastic modulus
N	number of loading cycles
$\boldsymbol{\varepsilon}$	strain tensor
$\mathrm{d}\boldsymbol{\varepsilon}_{\mathrm{e}}$	incremental elastic strain tensor
$\mathrm{d}\boldsymbol{\varepsilon}_{\mathrm{p}}$	incremental plastic strain tensor
f	yield surface function
$\Delta\gamma$	shear strain range
$\Delta\boldsymbol{\sigma}$	axial stress range
v	Poisson's ratio
$\boldsymbol{\sigma}$	stress tensor
$d\boldsymbol{\sigma}$	incremental stress tensor
σ_0	size of the yield surface
σ_{mean}	mean of the axial stress cycle

Ziegler (1959) and Mroz (1967) are inadequate for modeling ratcheting since they produce closed hysteresis loops. The nonlinear kinematic hardening rule by Armstrong and Frederick (1966) was found to over-predict ratcheting strain significantly under multiaxial loading. Several authors modified their model by introducing additional terms (Bower, 1989; Chaboche and Nouailhas, 1989a,b; Chaboche, 1991; Ohno and Wang, 1993a,b; Jiang and Sehitoglu, 1994a,b; McDowell, 1995). These new nonlinear kinematic hardening models can describe the hysteresis loop and uniaxial cyclic ratcheting well enough, but cannot predict multiaxial ratcheting responses satisfactorily. Also, as indicated by Bari and Hassan (2000, 2001), undesirable features in the predicted results of ratcheting strain still persist in most of these models.

Bari and Hassan proposed a modified kinematic hardening rule using the idea of Delobelle et al. (1995) in the framework of the Chaboche model. Since the Ohno–Wang model is regarded as a most successful, though still over-predictive, one among available models, this study will use the same constitutive framework and propose an improved kinematic hardening rule that incorporates the Burlet–Cailletaud radial evanescence term and the Delobelle parameter (δ') to control shakedown and over-prediction. An evolution equation for δ' will be proposed for correlation over a much larger number of cycles compared with other models in the literature. Ratcheting tests have been conducted on tubular specimens of S45C steel under the condition of four types of nonproportional axial–torsional loading. The model results will be compared with experimental data.

2. Ratcheting experiments

The material used in the study was medium carbon steel S45C (equivalent to AISI 1045 steel), which was acquired in the form of a round bar with a diameter of 32 mm. The material was held at 850 °C for 30 min

Table 1
Mechanical properties of S45C steel

σ_u (MPa)	σ_y (MPa)	τ_y (MPa)	RA(%)	δ (%)	E (GPa)	G (GPa)	v
798	590	320	39	17	205	79	0.298

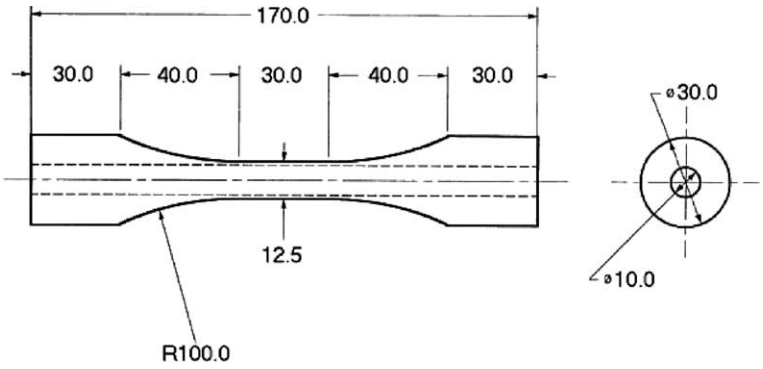

Fig. 1. Specimen geometry (dimensions in mm).

and water-quenched. It was then tempered at 600 °C in the furnace for 40 min and cooled in oil. The chemical composition of the material is (wt.%): C 0.43, Si 0.18, Mn 0.69, P 0.023, S 0.007. The mechanical properties are shown in Table 1.

The specimen used in this study, given in Fig. 1, has a tubular geometry with outside and inside diameters of 12.5 and 10 mm, respectively, in the gage section. Tests were conducted on an Instron tension–torsion machine using an axial–torsional extensometer mounted on the outside of the specimen gage section. Strains and stresses were recorded in the personal computer using an automated data acquisition system. All tests were conducted at room temperature under load control for axial loading and under strain control for torsional loading. The frequency of cyclic loading was 0.5 Hz. Triangular waveform was employed in the tests.

The loading paths in the axial stress–shear strain plane (σ–γ plane) used in ratcheting tests are illustrated in Fig. 2. The values of controlled parameters are given in Table 2. These tests consist of a constant amplitude shear strain cycling under a constant axial load (Case 1), (2) a constant amplitude proportional path with mean axial stress (Case 2), (3) a 90° out-of-phase path with mean axial stress (Case 3), and (4) a butterfly path with mean axial stress (Case 4). In all cases the shear strain amplitude was set at 0.866%.

In addition to the four axial–torsional tests, completely reversed, uniaxial and torsional tests were conducted at several strain amplitudes to obtain the cyclic stress–strain curves.

3. Description of the constitutive model

The total strain increment is decomposed into the elastic and plastic parts:

$$d\boldsymbol{\varepsilon} = d\boldsymbol{\varepsilon}_e + d\boldsymbol{\varepsilon}_p. \tag{1}$$

The material is assumed to follow the von Mises yield criterion, which is given by

$$f(\boldsymbol{\sigma} - \boldsymbol{\alpha}) = \left[\frac{3}{2}(\boldsymbol{s} - \boldsymbol{\alpha}) : (\boldsymbol{s} - \boldsymbol{\alpha})\right] = \sigma_0^2, \tag{2}$$

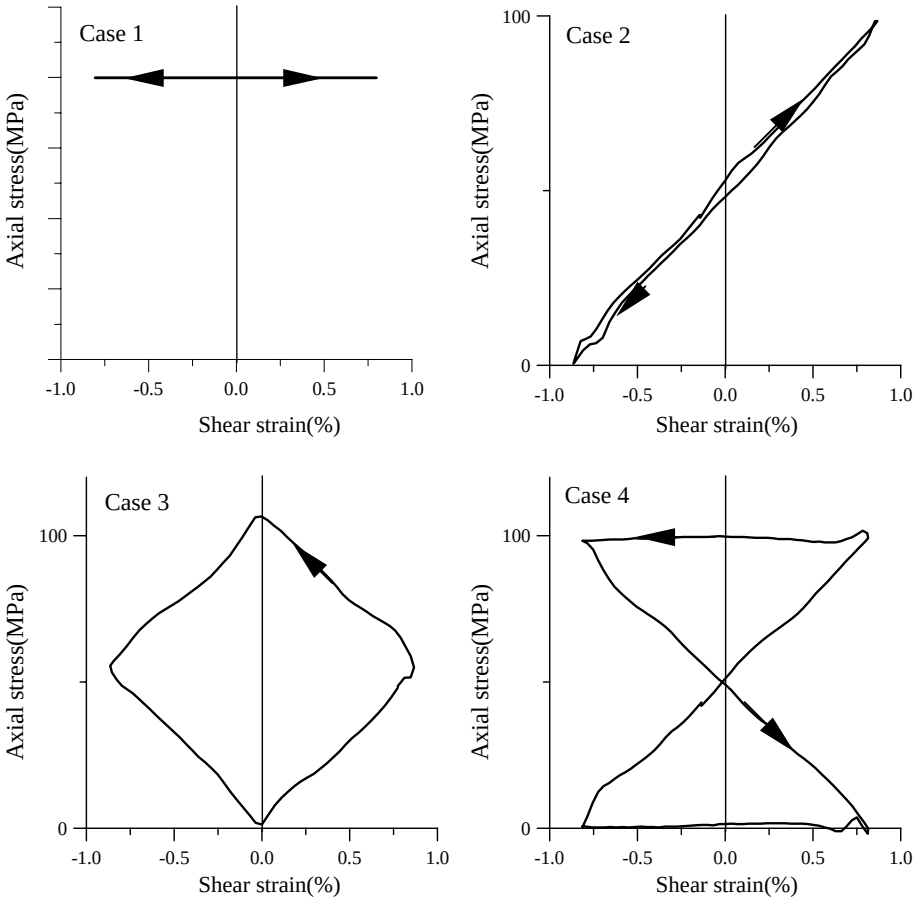

Fig. 2. Loading paths in ratcheting experiments.

Table 2
Summary of ratcheting experiments

Test no.	Loading path	$\Delta\gamma/2$ (%)	γ_{mean} (%)	$\Delta\sigma/2$ (MPa)	σ_{mean} (MPa)	$\Delta\tau/2$ (MPa)
1	Case 1	0.866	0	0	100	270
2	Case 2	0.866	0	50	50	239
3	Case 3	0.866	0	50	50	260
4	Case 4	0.866	0	50	50	274

where $\boldsymbol{s} = \boldsymbol{\sigma} - (\sigma_{kk}/3)\boldsymbol{I}$ is the deviatoric stress tensor, $\boldsymbol{\alpha}$ is the back stress, and σ_0 is the size of the yield surface, $\boldsymbol{I}$ is a unit tensor, and the inner product is defined by, e.g. $\boldsymbol{s} : \boldsymbol{t} = s_{ij}t_{ij}$.

The plastic flow can be stated as

$$\mathrm{d}\boldsymbol{\varepsilon}_{\mathrm{p}} = \frac{1}{H}\langle \mathrm{d}\boldsymbol{s} : \boldsymbol{n}\rangle \boldsymbol{n}, \tag{3}$$

where $\langle\ \rangle$ is the Macauley bracket: $\langle A\rangle = A$ if $A > 0$, $\langle A\rangle = 0$ otherwise.

3.1. The Ohno–Wang model

3.1.1. Model formulation

Ohno and Wang (1993a,b) used a multilinear model in which several kinematic hardening rules of the Armstrong–Frederick type are superposed. They assumed that each component of back stress $\boldsymbol{\alpha}_i$ has a critical state for its dynamic recovery term to be activated. The Ohno–Wang model can be written as follows:

$$\boldsymbol{\alpha} = \sum_{1}^{M} \boldsymbol{\alpha}_i,\ \mathrm{d}\boldsymbol{\alpha}_i = \gamma_i \left[\frac{2}{3} r_i \mathrm{d}\boldsymbol{\varepsilon}_{\mathrm{p}} - \left(\frac{\overline{\alpha_i}}{r_i} \right)^{m_i} \boldsymbol{\alpha}_i \left\langle \mathrm{d}\boldsymbol{\varepsilon}_{\mathrm{p}} : \frac{\boldsymbol{\alpha}_i}{\overline{\boldsymbol{\alpha}_i}} \right\rangle \right], \tag{4}$$

where, $\boldsymbol{\alpha}_i$ is the ith component of the deviatoric back stress $\boldsymbol{\alpha}$, $\overline{\alpha_i}$ is the magnitude of $\boldsymbol{\alpha}_i$, $\overline{\alpha_i} = \sqrt{3/2\boldsymbol{\alpha}_i : \boldsymbol{\alpha}_i}$, γ_i and r_i are material constants.

A sufficient number of decomposed hardening rules should be used in the Ohno–Wang model in order to produce a good representation of the stable uniaxial stress–strain hysteresis loop. In this study, eight decompositions are found sufficient.

3.1.2. Parameter determination

Parameters in the Ohno–Wang model are determined from the uniaxial cyclic stress–strain curve. The loading part of the stress–strain curve is divided into several segments as shown in Fig. 3. The parameters γ_i and r_i for each segment can be determined from the following equations:

$$\gamma_i = \frac{1}{\varepsilon_{\mathrm{p}(i)}}; \quad r_i = \left(\frac{\sigma_{(i)} - \sigma_{(i-1)}}{\varepsilon_{\mathrm{p}(i)} - \varepsilon_{\mathrm{p}(i-1)}} - \frac{\sigma_{(i+1)} - \sigma_{(i)}}{\varepsilon_{\mathrm{p}(i+1)} - \varepsilon_{\mathrm{p}(i)}} \right) \varepsilon_{\mathrm{p}(i)} \quad \text{for } i \neq 1, \tag{5}$$

and r_1 is determined using $\sum_1^M r_i + \sigma_0 = \sigma_{\max}$.

In Eq. (5) $\sigma_{(i)}$ and $\varepsilon_{\mathrm{p}(i)}$ denote the stress and plastic strain at the ith point on the stress–plastic strain curve as indicated in Fig. 3. The exponents, m_i, in Eq. (4) are assumed to be the same for all segments and should be determined from a uniaxial ratcheting experiment, as illustrated in Fig. 4.

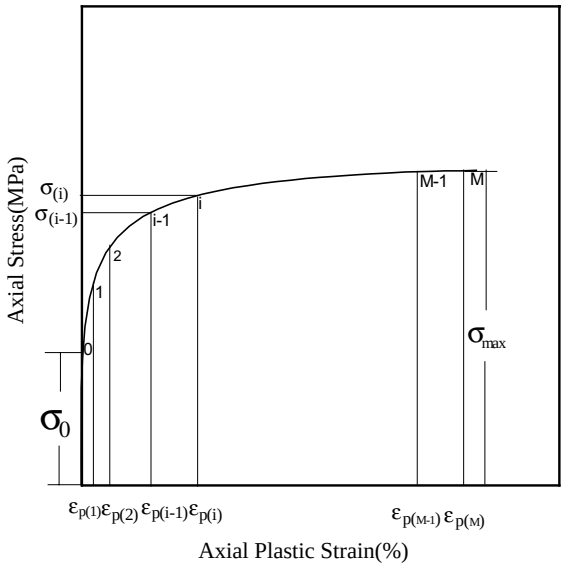

Fig. 3. Definition of parameters in the Ohno–Wang model from uniaxial stress–strain curve.

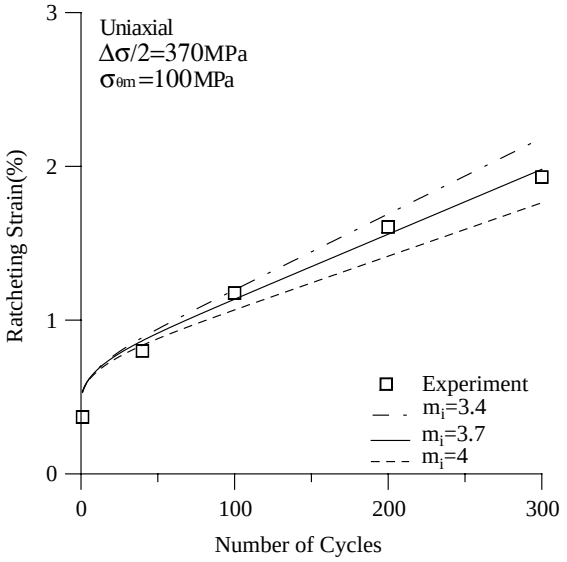

Fig. 4. Determination of parameter m_i in the Ohno–Wang model from uniaxial ratcheting experiment.

The Ohno–Wang model parameters used in this study for simulation of multiaxial ratcheting are:

$$\sigma_0 = 220 \text{ MPa}, \quad E = 187\,000 \text{ MPa}, \quad G = 90\,000 \text{ MPa},$$

$$\gamma_{1\text{–}8} = 2500, 1250, 666.7, 500, 333.3, 200, 125, 83.3,$$

$$r_{1\text{–}8} = 88, 42, 30.4, 21.3, 28.3, 31, 27.8, 76.4 \text{ MPa}, \quad m_i = 3.7 (i = 1, M).$$

3.1.3. Ratcheting simulation

Figs. 5 and 6 show experimental data and the results of simulations based on the Ohno–Wang model and the above set of parameter values. It has been known in ratcheting studies that the Ohno–Wang model can describe accurately the uniaxial and torsional hysteretic behavior but over-predicts biaxial ratcheting, though the degree of over-prediction is smaller than those of the Chaboche model and some modified models such as McDowell, Jiang and Sehitoglu (Bari and Hassan, 2002). The numerical results of this study verify again that the Ohno–Wang model does not yield good simulations of biaxial ratcheting. Furthermore, as the strain increases, the components of deviatoric back stress α_i reach their respective magnitudes of r_i and the dynamic recovery terms become fully operative. Each of the kinematic hardening rules is then the same as the Armstrong–Frederick kinematic hardening rule, and the rate of predicted ratcheting strain becomes constant. Therefore, the Ohno–Wang model cannot simulate the trend of decreasing ratcheting rates that occur in some experiments.

As indicated by some researchers (Jiang and Sehitoglu, 1996; Bari and Hassan, 2000), the over-prediction of biaxial ratcheting results from the fact that all parameters in the Ohno–Wang model are determined from uniaxial experiments and there is no parameter that can control the biaxial ratcheting behavior. Bari and Hassan (2002) modified the Chaboche model by adding the Delobelle kinematic hardening rule (Delobelle et al., 1995) and reported a considerable improvement in correlating multiaxial ratcheting data. Enlightened by their work, a similar approach has been attempted in this study within the framework of the Ohno–Wang model, which is outlined in what follows.

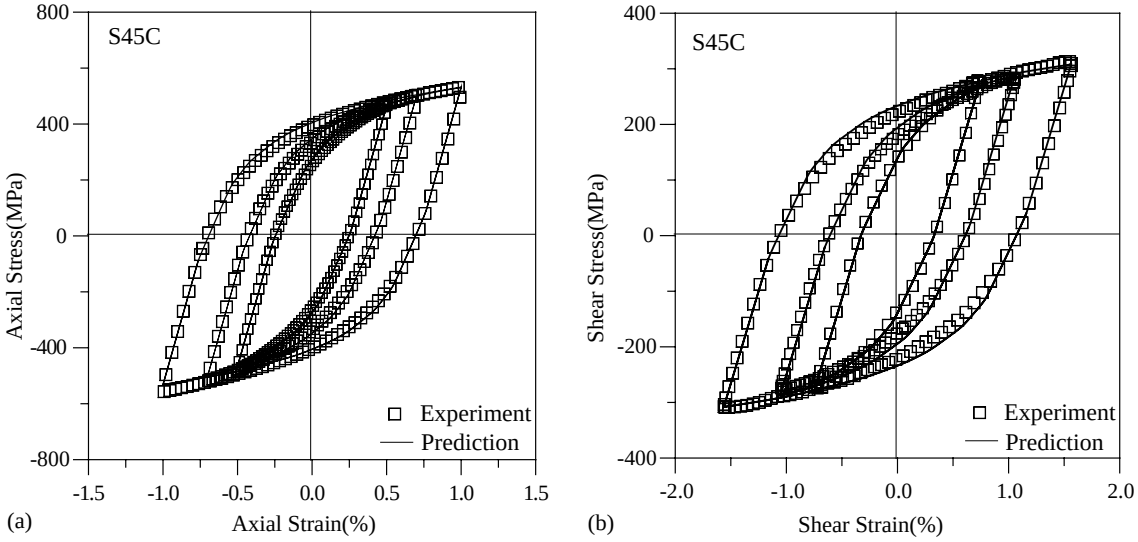

Fig. 5. Prediction of cyclic stable strain–stress curves from Ohno–Wang model: (a) uniaxial and (b) torsional.

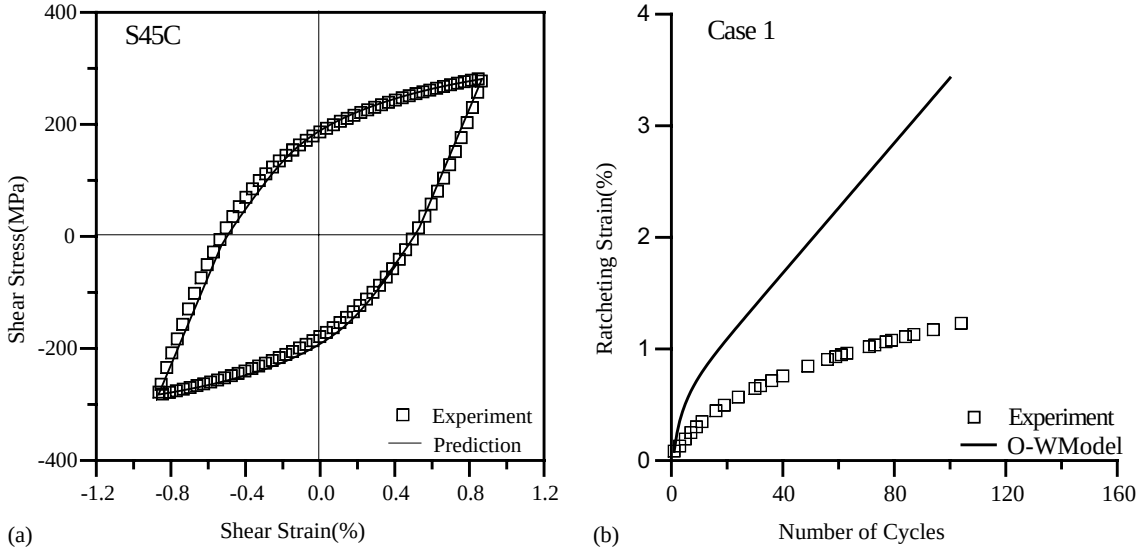

Fig. 6. Comparison of experimental data and predicted data by the Ohno–Wang model for Case 1: (a) shear stress–strain loop and (b) axial ratcheting strain.

3.2. An improved model

In order to simulate the uniaxial ratcheting experiments, Burlet and Cailletaud (1986) modified the radial evanescence term in the Armstrong and Frederick (1966) hardening rule in the following form:

$$\mathrm{d}\boldsymbol{\alpha} = \frac{2}{3}C\mathrm{d}\boldsymbol{\varepsilon}_{\mathrm{p}} - \gamma(\boldsymbol{\alpha} : \boldsymbol{n})\boldsymbol{n}\mathrm{d}p, \quad \boldsymbol{n} = \sqrt{\frac{2}{3}}\frac{\partial f}{\partial \boldsymbol{\sigma}} = \sqrt{\frac{2}{3}}\frac{(\boldsymbol{s}-\boldsymbol{\alpha})}{\sigma_{\mathbf{0}}}. \tag{6}$$

The plastic modulus expression obtained from this hardening rule by satisfying the consistency condition ($\dot{f} = 0$) is the same as that obtained from the Armstrong–Frederick hardening rule under uniaxial loading condition. The direction of $\boldsymbol{\alpha}$ is the same as that of $\boldsymbol{n}$, and hence the radial evanescence term ($\gamma(\boldsymbol{\alpha} : \boldsymbol{n})\boldsymbol{n}\mathrm{d}p$) is reduced to the dynamic recovery term of the Armstrong–Frederick hardening rule. In addition, since the simulation of uniaxial ratcheting depends entirely on the calculation scheme of the plastic modulus, these two rules produce the same results; while for biaxial loading, the radial evanescence term ($(\boldsymbol{\alpha} : \boldsymbol{n})\boldsymbol{n}\mathrm{d}p$) of the Burlet–Cailletaud rule essentially yields a tensor along the plastic strain-rate direction, and thus the results become similar to those of the Prager linear hardening rule that predicts shakedown ratcheting (Bari and Hassan, 2002). In order to compromise over-prediction of the Ohno–Wang model and shakedown of the Burlet–Cailletaud model, this study makes use of the Delobelle et al.'s scheme (1995) in the following manner:

$$\mathrm{d}\boldsymbol{\alpha}_i = \gamma_i\left\{\frac{2}{3}r_i\mathrm{d}\boldsymbol{\varepsilon}_{\mathrm{p}} - \left(\frac{\overline{\alpha_i}}{r_i}\right)^{m_i}[\delta'\boldsymbol{\alpha}_i + (1-\delta')(\boldsymbol{\alpha}_i : \boldsymbol{n})\boldsymbol{n}]\left\langle \mathrm{d}\boldsymbol{\varepsilon}_{\mathrm{p}} : \frac{\boldsymbol{\alpha}_i}{\overline{\alpha_i}}\right\rangle\right\}, \quad i = 1, 2, \ldots, M, \tag{7}$$

where, γ_i, r_i, m_i and $\overline{\alpha_i}$ are the same as those of the Ohno–Wang model, Eq. (4). The parameter δ' is called the Delobelle parameter in this study. When $\delta' = 0$, the modified hardening rule is reduced to the Burlet–Cailletaud model that predicts shakedown ratcheting; while $\delta' = 1$, it reverts to the Ohno–Wang model (see Fig. 7).

Following the consistency condition ($\dot{f} = 0$), the plastic modulus is expressed as follows:

$$H = \sum_{1}^{M}\gamma_i\left\{\frac{2}{3}r_i - \sqrt{\frac{2}{3}}\left(\frac{\overline{\alpha_i}}{r_i}\right)^{m_i}(\boldsymbol{\alpha}_i : \boldsymbol{n})\left\langle \frac{\mathrm{d}\boldsymbol{\varepsilon}_{\mathrm{p}}}{\mathrm{d}p} : \frac{\boldsymbol{\alpha}_i}{\overline{\alpha_i}}\right\rangle\right\}, \quad \mathrm{d}p = \sqrt{\frac{2}{3}\mathrm{d}\boldsymbol{\varepsilon}_{\mathrm{p}} : \mathrm{d}\boldsymbol{\varepsilon}_{\mathrm{p}}}. \tag{8}$$

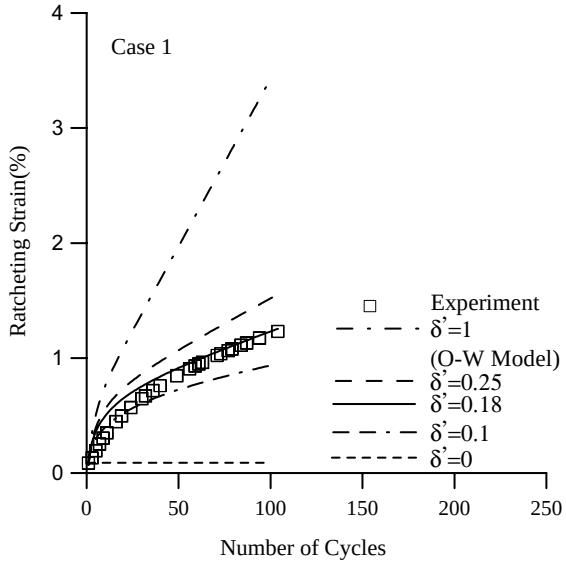

Fig. 7. Prediction of ratcheting strain by the modified model with different values of δ'.

From Eq. (8) one can see that the plastic modulus expression (H) does not include δ'. Therefore, it can be stated that δ' can only be determined from a biaxial ratcheting response, that is to say, δ' can influence biaxial ratcheting responses without any effect on the plastic modulus and uniaxial ratcheting responses. It also implies that all of the parameters of the Ohno–Wang model can be used with the modified hardening rule.

The simulations with the modified model using a constant δ' are presented in Fig. 7. The modified model appears to simulate the biaxial ratcheting response reasonably well with a proper choice of δ' for a relatively low number of cycles. However, as observed in Fig. 8(a), the ratcheting strain rate tends to be decreasing

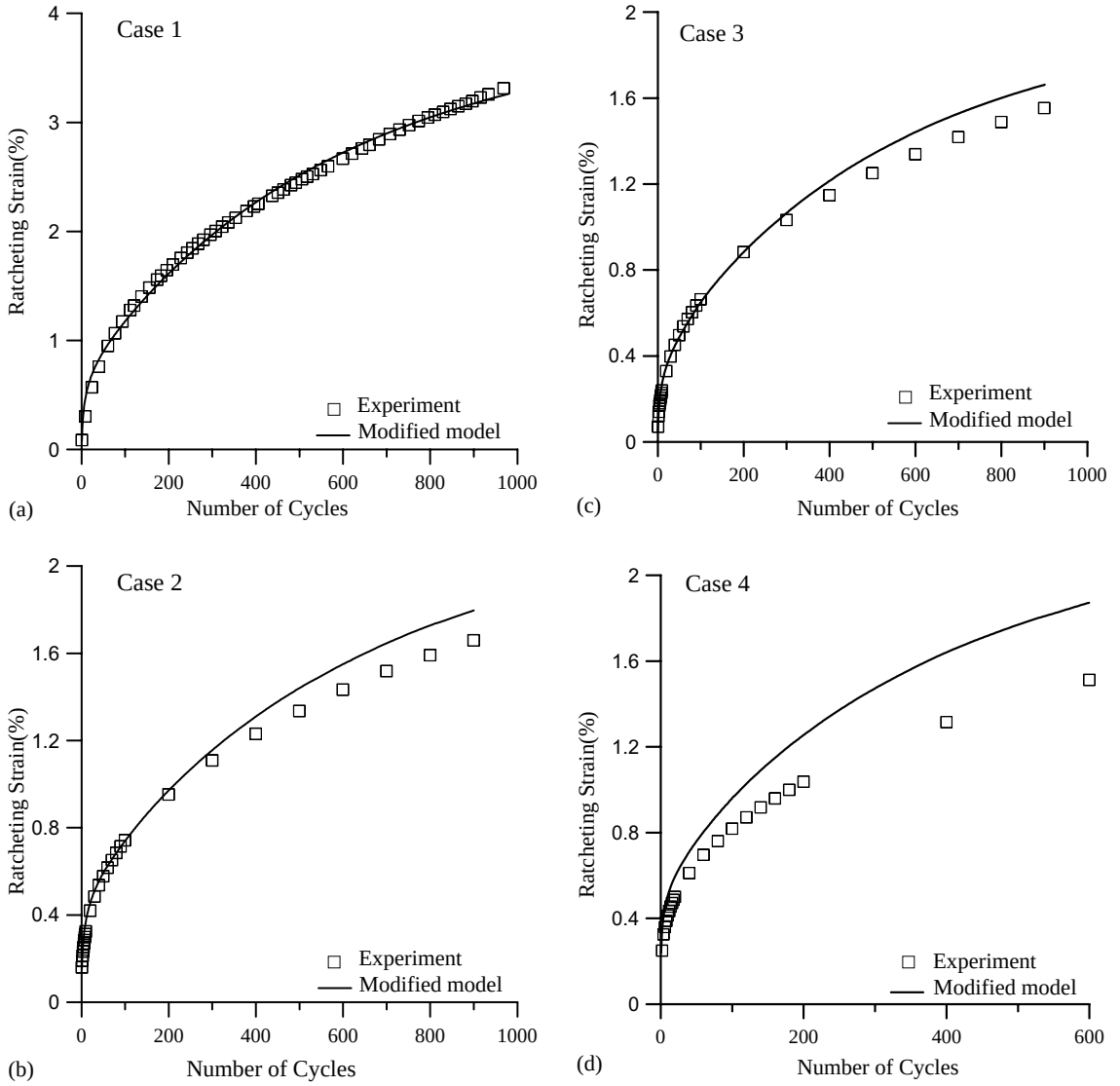

Fig. 8. Comparison of experimental ratcheting strain with predictions by the modified model with evolutionary δ': (a) Case 1, (b) Case 2, (c) Case 3 and (d) Case 4.

with the increasing number of cycles. The modified model with a constant δ' cannot reflect this trend very well as the number of cycles becomes large. From numerical computations and the results shown in Fig. 7, a conclusion can be drawn that the smaller δ', the smaller the ratcheting strain rate of the model prediction becomes. In order to provide a decreasing ratcheting strain rate with the increasing number of cycles, it is necessary to generate an evolution function for δ' monotonically decreasing with the number of cycles. An evolution function of δ' is proposed as follows:

$$\mathrm{d}\delta' = \beta(\delta'_{\mathrm{st}} - \delta')\mathrm{d}p, \tag{9}$$

where δ'_{st} is the saturated value of δ' and β is an evolution coefficient.

The initial value of δ' is denoted by δ'_0. The value of δ'_{st} is sensitive to the slope of ratcheting strain at large cycles, δ'_0 is closely related to the ratcheting rates of initial cycles, and β decides the evolution of the ratcheting strain rate. The values of δ'_{st}, δ'_0 and β can be estimated from the biaxial ratcheting curves, say Fig. 8(a). For medium carbon steel S45C, these values were taken as: $\delta'_{\mathrm{st}} = 0$, $\delta'_0 = 0.18$, $\beta = 0.16$. The effects of δ'_{st}, δ'_0 and β on the ratcheting strain rate are further discussed in a separate paper (Chen and Jiao, submitted for publication).

The proposed kinematic hardening rule has been used in this study with the evolution equation for δ' and the parameter values of the Ohno–Wang model given earlier.

4. Results and discussion

The modification on the Ohno–Wang model made in this study is not effective for uniaxial ratcheting since the radial evanescence term is reduced to the dynamic recovery term of the Armstrong and Frederick (1966) hardening rule. The uniaxial ratcheting prediction was satisfactory to 300 cycles (see Fig. 4) with $m_i = 3.7$, however the model increasingly overpredicted actual ratcheting after that; for instance 30% off at 400 cycles.

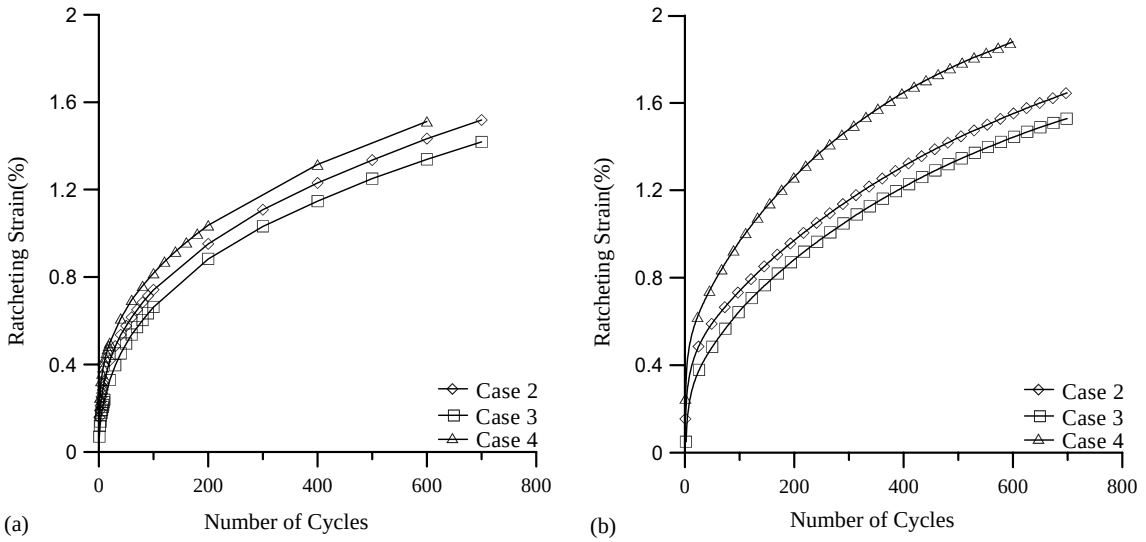

Fig. 9. Ratcheting strain for different loading paths with the same mean stress and amplitude of torsional strain: (a) experiments and (b) predictions.

The ratcheting predicted by the modified model under biaxial loading was compared with experimental data for Cases 1–4 in Fig. 8. It is found that predictions are in reasonably good agreement with experimental data. It is remarked here that the correlation lasted to a large number of cycles close to the termination of the tests, while currently available models have been validated only for a relatively small number of cycles. For Case 1, from which the new parameter δ' has been determined, the agreement is naturally found best. However, other cases are also found in good correlation when compared with other multiaxial ratcheting studies.

A comparison of experimental ratcheting strain for the three tests with the same mean axial stress and amplitude of torsional strain, Cases 2–4, shows the effect of loading paths on the ratcheting strain (Fig. 9(a)). The numerical results in Fig. 9 (b) for the corresponding cases indicate that the modified model can also predict the order of magnitudes of the ratcheting strain correctly under different loading paths. Predictions of the cyclic shear stress–strain response and the axial vs. shear stress response under nonproportional loading of Case 3 are shown in Fig. 10. Fig. 11 gives the axial vs. shear stress loops for Case 4. The good agreement with experimental data in these figures demonstrates that the modified model can simulate multiaxial responses under axial–torsional loading, which helps validate rationality of the proposed plasticity model incorporating ratcheting responses.

McDowell (2000) attributed existing plasticity models' poor predictive capability to not accounting for microstructural deformation mechanisms. Bari and Hassan (2001) suggested that it would be needed to introduce anisotropy into the yield surface to enhance the predictive capability of ratcheting strain beyond the current assumption of invariant yield surface shape. Vincent et al. (2002) introduced a distortion model of subsequent yield surfaces into nonlinear kinematic hardening constitutive equations to describe multiaxial ratcheting.

While the approach taken in this paper may be considered as substantial improvement of ratcheting simulation, efforts are certainly needed for more reliable predictions. The materials and loading conditions used to verify the present model are limited. More comprehensive verification remains as a future work.

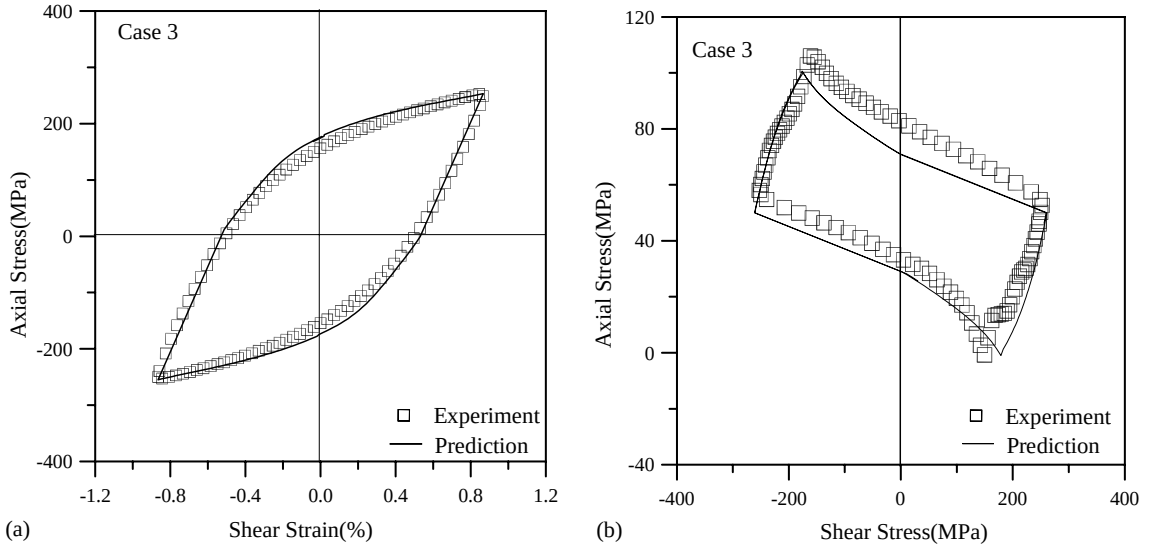

Fig. 10. Comparison of predicted and experimental data for Case 3: (a) shear stress–shear strain response and (b) axial stress–shear stress response.

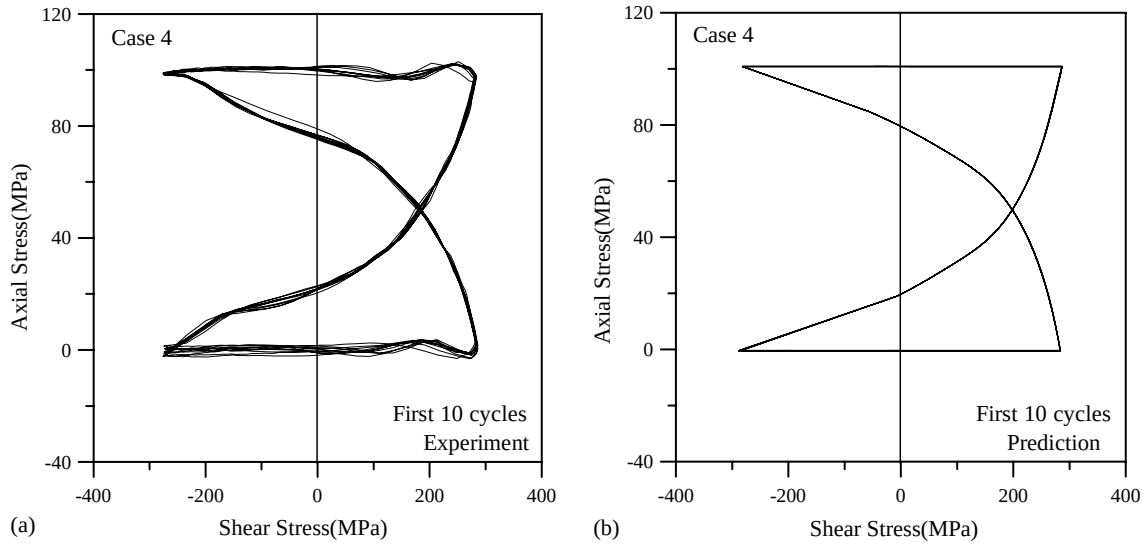

Fig. 11. Axial vs. shear stress response in the first 10 cycles for Case 4: (a) experiment and (b) prediction.

5. Conclusions

Ratcheting tests were conducted on S45C steel for four nonproportional loading paths. A modified kinematic hardening rule that incorporates the Burlet–Cailletaud hardening rule and the Delobelle parameter δ' within the framework of the Ohno–Wang model has been proposed. All parameters except δ' of the modified model are the same as those of the Ohno–Wang model. δ' may be considered as a constant to describe the ratcheting responses at a relatively small number of cycles. In order to improve the simulation of ratcheting responses at large cycles, an evolution equation for δ' has been introduced. Material constants in the evolution equation can be determined from a biaxial ratcheting response, an example of which has been given in this study. Ratcheting simulations for the four types of loading paths are in good agreement with experimental data over a large number of cycles. The results indicate that the proposed model is a substantial improvement of multiaxial ratcheting prediction methods currently available in the literature.

Acknowledgements

The authors gratefully acknowledge financial support for this work, in part from the BK 21 Program at Pohang University of Science and Technology, and in part from National Natural Science Foundation of China and TRAPOYT.

References

Armstrong, P.J., Frederick, C.O., 1966. A mathematical representation of the multiaxial Bauschinger effect, CEGB Report RD/B/N731. Berkeley Nucl. Lab.

Bari, S., Hassan, T., 2000. Anatomy of coupled constitutive model for ratcheting simulation. Int. J. Plasticity 16, 381–409.

Bari, S., Hassan, T., 2001. Kinematic hardening rules in uncoupled modeling for multiaxial ratcheting simulation. Int. J. Plasticity 17, 885–905.

Bari, S., Hassan, T., 2002. An advancement in cyclic plasticity modeling for multiaxial ratcheting simulation. Int. J. Plasticity 18, 873–894.

Bower, A.F., 1989. Cyclic hardening properties of hard-drawn copper and rail steel. J. Mech. Phys. Solids 37, 455–470.

Burlet, H., Cailletaud, G., 1986. Numerical techniques for cyclic plasticity at variable temperature. Engng. Comput. 3, 143–153.

Chaboche, J.L., 1991. On some modifications of kinematic hardening to improve the description of ratcheting effects. Int. J. Plasticity 7, 661–678.

Chaboche, J.L., 1994. Modeling of ratchetting: evaluation of various approaches. Eur. J. Mech. A/Solids 13, 501–518.

Chaboche, J.L., Nouailhas, D., 1989a. Constitutive modelling of ratchetting effects. Part I: Experimental facts and properties of classical models. ASME J. Engng. Mat. Technol. 3, 384–390.

Chaboche, J.L., Nouailhas, D., 1989b. Constitutive modeling of ratchetting effects. Part II: Possibilities of some additional kinematic rules. ASME J. Engng. Mater. Technol. 3, 409–416.

Chen, X., Jiao, R., submitted for publication. Modified kinematic hardening rule for multiaxial ratcheting prediction. Int. J. Plasticity, accepted.

Delobelle, P., Robinet, P., Bocher, L., 1995. Experimental study and phenomelogical modelization of ratcheting under uniaxial and biaxial loading on an austenite stainless steel. Int. J. Plasticity 11, 295–330.

Hassan, T., Corona, E., Kyriakides, S., 1992. Ratcheting in cyclic plasticity. Part II: Multiaxial behavior. Int. J. Plasticity 8, 117–146.

Hassan, T., Kyriakides, S., 1992. Ratcheting in cyclic plasticity. Part I: Uniaxial behavior. Int. J. Plasticity 8, 91–116.

Hassan, T., Kyriakides, S., 1994a. Ratcheting of cyclically hardening and softening materials. Part I: Uniaxial behavior. Int. J. Plasticity 10, 149–184.

Hassan, T., Kyriakides, S., 1994b. Ratcheting of cyclically hardening and softening materials. Part II: Multiaxial behavior. Int. J. Plasticity 10, 185–212.

Jiang, Y., Sehitoglu, 1994a. Cyclic ratchetting of 1070 steel under multiaxial stress state. Int. J. Plasticity 10, 579–608.

Jiang, Y., Sehitoglu, H., 1994b. Multiaxial cyclic ratchetting under multiple step loading. Int. J. Plasticity 10, 849–870.

Jiang, Y., Sehitoglu, H., 1996. Modeling of cyclic ratcheting plasticity. Part 1: Development of constitutive relations. J. Appl. Mech. 63, 720–725.

McDowell, D.L., 1994. Description of nonproportional cyclic ratcheting behavior. Eur. J. Mech. A/Solids 13, 593–604.

McDowell, D.L., 1995. Stress state dependence of cyclic ratcheting behavior of two rail steels. Int. J. Plasticity 11, 397–421.

McDowell, D.L., 2000. Modeling and experiments in plasticity. J. Solids Struct. 37, 293–309.

Mroz, Z., 1967. On the description of anisotropic work hardening. J. Mech. Phys. Solids 15, 163–175.

Ohno, N., Wang, J.-D., 1993a. Kinematic hardening rules with critical state of dynamic recovery. Part I: Formulations and basic features for ratcheting behavior. Int. J. Plasticity 9, 375–390.

Ohno, N., Wang, J.D., 1993b. Kinematic hardening rules with critical state of dynamic recovery. Part II: Application to experiments of ratchetting behavior. Int. J. Plasticity 9, 391.

Ohno, N., 1998. Recent progress in constitutive modelling for ratchetting. Mater. Sci. Res. Int. 3, 1–9.

Portier, L., Calloch, S., Marquis, D., Geyer, P., 2000. Ratchetting under tension–torsion loadings: experiments and modeling. Int. J. Plasticity 16, 303–335.

Prager, W., 1956. A new method of analyzing stresses and strains in work hardening plastic solids. J. Appl. Mech. 23, 493–496.

Vincent, L., Colloch, S., Kurtyka, T., Marquis, D., 2002. An improvement of multiaxial ratcheting modeling via yield surface distortion. ASME Trans. J. Engng. Mater. Technol. 124, 402–411.

Ziegler, H., 1959. A modification of Prager's hardening rule. Quart. Appl. Math. 17, 55–65.